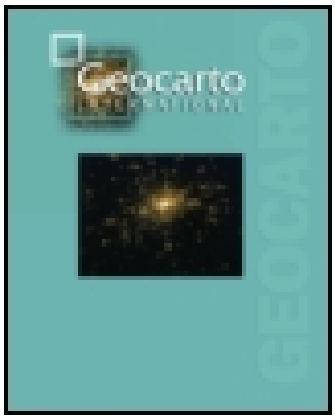

Geocarto International
Publication details, including instructions for authors and subscription information:
http://www.tandfonline.com/loi/tgei20

The application of remote sensing data to diagnose soil degradation in the Dakhla depression - Western Desert, Egypt

Mohamed E. Hereher[a] & Hossam Ismael[b]
[a] Department of Environmental Sciences, Faculty of Science, Damietta University, Egypt
[b] Geography Department, Faculty of Arts, Assuit University, New Valley, Egypt
Accepted author version posted online: 08 Jun 2015.

Publisher: Taylor & Francis
Journal: *Geocarto International*
DOI: http://dx.doi.org/10.1080/10106049.2015.1059901

The application of remote sensing data to diagnose soil degradation in the Dakhla depression - Western Desert, Egypt

Mohamed E. Hereher[1] **and Hossam Ismael**[2]
1-Depertment of Environmental Sciences, Faculty of Science, Damietta University, Egypt
2-Geography Department, Faculty of Arts, Assuit University, New Valley, Egypt
Email: mhereher@yahoo.com

Abstract
Dakhla depression in Egypt's Western Desert is experiencing two soil degradation processes, notably: soil salinization and sand encroachment. The present study aimed to diagnose the severity of these processes using remote sensing. Soil salinity was determined by spectral regression analysis between tasseled cap (TC) spectral transform extracted from a Landsat-8 image acquired in September 2013 along with synchronized soil salinity measurements. Assessment of sand advance rate was conducted by temporal change detection of brilliant crescentic sand dunes visualized by Google Earth in old (2002) and recent (2013) images. Results showed that salinized soils (dS/m4<) represent 91% of bare lands and salinization is attributed to aridity, topography and poor drainage. Barchan dunes north and south of Abu Tartur escarpment moved at rates of 5.9 and 3.6 m/y, respectively. The escarpment protected the majority of the depression from massive dune invasion. However sand encroachment is clearly observed west of the depression.

Keywords: Arid lands, sand drift, salinization, desertification, Dakhla

1. Introduction

Arid lands are defined as the regions, in which the ratio between the annual precipitation to potential evapotranspiration (P/ET) ranges from 0.05 to 0.2 (UNEP, 1992). In north Africa, arid lands represent more than 95% of the terrain area (Tolba, 1986) except for the littoral zone of the Mediterranean Sea. Arid lands are literally vulnerable to soil degradation by the drought conditions. Due to the scant rainfall and high evaporation rates, there is a likelihood for salts to build up in the soil profile to the degree that can threat plant growth and even destroy the soil profile structure. In some circumstances soil degradation could be as severe as the biological functions of the ecosystem are impaired and desertification conditions prevail (Sumner, 2000). Kassas (1987) reported that manifestations of desertification in arid lands include soil salinization and sand encroachment. Salinization is a significant process of soil

degradation (UNEP, 1991). Primary salinization develops as a result of climatic, geologic, and topographic factors, while secondary salinization occurs as a result of human activities pertaining to mal-management of water resources, such as inefficient irrigation/drainage practices and poor soil management. Chhabra (1996) reported that the main sources of salts within the soil profile are: 1- soil weathering; 2- irrigation with inadequate drainage; 3- irrigation with saline water; 4- shallow water table; 5- fossil salts; 6- seepage from up-slopes containing salts; 7- Ocean and 8- chemical fertilizers.

Conventional field inventory methods of salt-affected soils are generally labor intensive, expensive and time consuming particularly for regional surveying (Dwivedi, 1992). Remote sensing affords a cost-effective and synoptic technique for mapping salt-affected soils and environmental monitoring (Metternicht & Zink, 2003, Elmahdy & Mohamed 2015a&b, Elmahdy et al. 2015). Information about the extent of salt-affected soils could be directly extracted from remote sensing of salt efflorescence and salt crust or indirectly by monitoring vegetation stresses using vegetation indices (Mougenot et al., 1993). In some cases, salt-affected soils and sabkhas could be distinguished in satellite images by their high albedo, particularly if white salts are accumulated at the surface. However, it is usually hard to recognize low salt concentrations from satellite data (Hereher et al., 2010). In all cases, salinized soils have a strong reflection in the visible and near-infrared spectral bands; the higher the degree of soil salinity, the more the reflection in these spectra (Rao et al., 1995). Recent trends of remote sensing involve the use of hyper-spectral data and sub-pixel spectral mixture analysis as promising techniques for mapping salt-affected soils and discriminating individual salt type. Nevertheless, the limited availability of hyper-spectral data is a potential constraint for their general use on a regional scale (Judkins & Myint, 2012). On the other hand, the Landsat images are quite available free of charge for any region in the world and are provided by the United States Geological Survey (USGS). These images have a reasonable spectral resolution including visible, near infrared (NIR), shortwave infrared (SWIR) and thermal infrared (TIR) bands that are suitable for extracting useful information about salt-affected soils (Metternicht & Zink, 2003). Although the spatial resolution (30 m) is somewhat moderate, it is equitable for regional assessment of soil salinity. Moreover, there is numerous previous studies operated Landsat images to detect soil salinity by image

classification and spectral indices (Dwivedi & Rao, 1992; Fernandez-Bucesa et al., 2006; Masoud & Koike, 2006). Regression correlations are being effective and acceptable techniques for mapping salinity in a regional basis (Judkins & Myint, 2012). In Egypt delineation of salt-affected soils using remote sensing is an ongoing pursuit since 1990s (Sadek, 1993; Darwish & Abdel Kawy, 2008; Hereher et al., 2010; Mohamed et al., 2011; Nawar et al., 2014).

Mobile sand dunes are considered a significant problem in arid regions, where they encroach on road networks, agricultural lands and residential areas (Knight et al. 2004). In terms of dune activity, Tchakerian (1999) identified three types of dunes: active; dormant and relict dunes. Active dunes are the most hazardous as they occur in areas of significant sand supply and void of vegetation (Lancaster, 2009). Aeolian sands constitute about 16% of Egypt area, mostly in the Western Desert (Misak and Draz, 1997) as major sand deposits (sand seas and dune fields) occur west of the Nile Valley. Quantification of sand movement ranges from field measurements of sand drift using sand traps (Fryberger et al., 1984) through calculations of sand fluxes using empirical equations (Livingstone et al., 2007) to assessment of dune activity from climatic data (Hereher, 2014). Remote sensing techniques have provided indispensible tools for tracking dune movements in remote and inaccessible sandy deserts (Hugenholtz et al., 2012). They are considered more accurate than conventional field measurements as well as empirical assessment because satellite data synoptically delineate the change in the morphology and location of dunes in old and recent images (Yao et al., 2007). Moderate resolution satellite data, such as Landsat TM and ETM+ images are quite appropriate for mapping temporal changes of large sand dunes during the last 40 years (Hereher, 2010), while finer resolution data, such as Quickbird images, which are visualized by Google Earth afford a global panorama coverage for the dynamics of small sand dunes since the last decade (Sparavigna, 2013). Mapping dune advance in Google Earth was applied along the Nile Valley east of the study area (Hereher, 2014).

The present study aims to explore the effectiveness of using remote sensing to diagnose soil degradation status in the Dakhla depression, Western Desert of Egypt as one of the promising regions for agricultural development in the country. Soil degradation processes analyzed in the present study include soil salinization and dune encroachment. Regression analysis and temporal change assessment were the

techniques applied to achieve the goals of the study. Topographic influence upon soil salinization and dune types as well as dune encroachment is a target to be investigated in the present study.

2. The study area

Dakhla (the inner in Arabic) is a NW longitudinal depression located within the southern part of the Western Desert of Egypt (Lat. 25° 25' 56" N to 25° 55' 11" N and Long. 29 22 14 E to 28 28 37 E). It is far away about 350 km west of the Nile River and 750 km southwest of Cairo (Fig. 1). The depression extends to about 80 km in the east-west direction and about 30 km in the north-south direction. Dakhla depression is bordered from the north by a limestone escarpment known as Abu Tartur plateau, which rises to about 500 m above the sea level (asl). The southern side of the depression rises gradually southward until the mean level of the desert. The region is extremely arid as it is a part of the hot and dry Sahara, where descending air coming from the equatorial region produces a stable hot airmass known as the tropical continental region (Beaumont, 1993). Climatic parameters of Dakhla (Table 1) reveal that the region is very dry. Average annual temperatures range from 12°C in January to 31°C in July. Evapotranspiration rates are as high as 2.6 mm/d in January and up to 9.1 mm/d in June. Annual precipitation does not exceed 1 mm and rainy months are January and February (CLAC, 2015). Wind speed ranges from 3 knots in December to 5.5 knots in June and the predominant wind direction is the north-northwest. There is a massive sand dune field; the Great Sand Sea, that extends to about 400 km north of the Dakhla depression. The majority of the population in Dakhla (about 70,000 persons) are working in farming and grazing. Water recourses are exclusively restricted to groundwater recharged from the Nubian sandstone aquifer system. It is planned to restrain 200,000 persons in the depression relying on the groundwater reserves. Perennial vegetation is the date palm, however, vegetables, alfalfa and rice are also cultivated. Soils of the Dakhla depression is classified as *Calcisols* (FAO/UNESCO, 1977).

3. Materials and methods

3.1 Satellite data

To delineate soil salinization conditions in the Dakhla depression, one satellite image from the Landsat-8 operational land imager (OLI) was obtained from the USGS Earth Explorer gateway (http://earthexplorer.usgs.gov/). The image was

acquired in September 11, 2013 just few months after the launch of this most recent generation of the Landsat series. The image (path 177, row 42) has 28.5 m spatial resolution and 11 spectral bands including visible (4 bands), NIR (1 band), SWIR (2 bands) and TIR (2 bands) of the spectrum. For mapping the change in dune movement, fine resolution satellite images displayed by Google Earth were visually examined to map locations of prominent crescentic dunes in the region as appear in 2002 and 2013. In addition, a digital elevation model (DEM) from the Shuttle Radar Topography Mission (SRTM) was acquired for the region in order to highlight topographic variation along the depression with regard to surrounding desert landforms. The DEM is a single band image in 90 m spatial resolution and 1 m vertical resolution assigned to the UTM projection. The SRTM image was obtained from the Global Land Cover Facility of the University of Maryland, USA (http://www.landcover.org/index.shtml).

3.2 Image pre-processing

Image pre-processing includes geometric and atmospheric correction of the OLI image. Geometric correction was carried out using image to image rectification procedures through a first order polynomial transform algorithm. The master images was a geo-referenced Landsat-5 image acquired in 1984 from which the OLI image was rectified. It was crucial to have a geo-rectification accuracy of less than one pixel in the Landsat-8 image. The OLI images was assigned to the Universal Transverse Mercator (UTM) projection. The atmospheric correction was carried out by applying the COST Model in ERDAS Imagine using the dark-object subtraction method proposed by Chavez (1996). As the OLI image was processed individually, then no need to further radiometric correction. Although there are 11 spectral bands in the Landsat-8 OLI image, only six bands were selected and stacked together to generate a new image for soil salinization assessment, in the following order of bands: B1 (blue), B2 (green), B3 (red), B4 (NIR), B5 (SWIR1) and B6 (SWIR2). SWIR1 and SWIR2 bands have a wavelengths of 1.56 - 1.66 µm and 2.10 - 2.30 µm, respectively.

3.3 Image processing

The extent of cultivated lands within the entire depression was estimated in 2013 using the OLI image by applying the soil adjusted vegetation index (SAVI) (Huete, 1988), which was designed to highlight green vegetation using the following formula: SAVI = [(NIR - R)/(NIR + R + L)] x (1 + L), where NIR and R are the

reflectance in the near infrared and red spectra, respectively. The constant L is an empirical value (0.5) that compensates for the soil background effect. This index was preferred to the most famous normalized difference vegetation index (NDVI) (Tucker, 1979) because it takes into consideration the impact of the soil background on each pixel reading in the image. The extent of the green vegetation was determined after assigning a threshold value, beyond which all the pixels were counted as agricultural land. The SAVI threshold value is 0.1, hence, all pixels equal or greater than 0.1 were grouped and counted as cultivated lands. SAVI was applied in a similar study south of the Dakhla depression, where salinized soils exist near cultivated lands (Hereher, 2015). The DEM was utilized to perform a painted relief image for the study area in order to elucidate the relative depths of the depression in relation to the surrounding plateaus using ArcMap Software. Four elevation intervals above the sea levels (< 150 m; 150-300; 300-450 and >450 m) were highlighted.

3.4 Soil sampling and regression analysis

During September 2013 (the same time of image acquisition), a total of 66 representative soil samples were collected (at 10 cm depth from the surface) from the entire Dakhla depression with the aid of a hand-held GPS instrument (Fig. 2). Sampling locations were designed to represent bare soils and fallow agricultural lands and to avoid actively cultivated farmlands. Soil samples were dried in the air and gravel size particles were excluded using a 2-mm sieve. A soil paste (1W:1V) was prepared for each sample and the EC of the soil extract was determined according to Dellavalle (1992) using a bench-top EC meter and salinity was expressed in dS/m. Soil texture of each sample was determined using the standard hydrometer method (Piper, 1955). A regression relationship analysis was conducted using the salinity value of each point and the corresponding spectral data of the same pixel within the six stacked bands in the OLI image. Eighteen regression relationships were performed using the individual digital numbers (B1 to B6) through band algebra and band transformations. The band transformations attempted were: band ratios (B3/B4, B4/B3, B3/B5, B5/B3, B3/B6 and B6/B3), band multiplication (B1*B3, B3*B4, B3*B6) spectral indices (B5-B3/B5+B3, B6-B1/B6+B1), and the TC transform. As the TC consists of brightness, greenness and wetness components, the first transform, which correlates with the bright soil was applied. The TC brightness component is calculated as: TC = 0.3037(B1)+0.2793(B2)+0.4743(B3)+0.5585(B4)+0.5082(B5)+

0.1863(B7) (Kauth & Thomas, 1976). The operated bands and their algebra were selected depending on the previous recommendations in the literature for their high correlation with saline soils (Dwivedi & Rao, 1992). Regression relationships were expected to reveal different correlation coefficients (R^2) and the highest R^2 equation was used to prepare a salt-affected soil map using the six-bands OLI image. The *Spatial Modeler* in ERDAS Imagine was operated to run the model and to produce a thematic map of soil salinity for Dakhla expressed in dS/m. Salinity values were sliced by *classification* tool in ArcMap into five EC classes: < 4 dS/m, 4-12 dS/m, 12-20dS/m, 20-28 dS/m, and >28 dS/m. Soils with EC < 4dS/m are considered non-saline (Chhabra, 1996).

3.5 Tracking sand dune movements

Tow sand dune fields, one north of the Dakhla depression and the other within the depression, were chosen to track changes in the locations of brilliant barchan dunes (Fig. 2). This type of dunes is easily distinguishable in satellite data as it appears as a crescent-shape with its horns occurring in the downwind direction. It also differs from the famous linear dune type that runs parallel to the dominant wind direction (Breed & Grow, 1979). The locations of the two dune fields were intentionally chosen to examine the impact of Abu Tartur Plateau upon the rate of dune movements. Google Earth was used to locate the position of the selected dunes in recent (2013) and in older (2002) images. Google Earth was displayed at a scale of 1:5000 and a selected dune from each dune field was monitored in the two dates. The displacement of each barchan dune was measured using the *ruler tool* in Google Earth. The annual rate of dune advance was estimated for the two dune fields.

4. Results

The shaded relief map derived from the DEM shows that the Dakhla is dotted by three micro-depressions within the Western Desert (Fig. 3). These micro-depressions locally known as Balat at the east; Al-Mauhoub/Mut at the middle; and Al-Mauhoub West at the western side. The three hollows forming the Dakhla depression have a total area of 1240 km^2, where they occur at a level below the contour line of 150 m (asl). The lowest point in the depression occurs at 92 m (asl) in the middle hollow (Mut), where an artificial lake -Lake Mut- was naturally formed from agricultural drainage. The northern escarpment occurs at more than 450 m (asl) and runs in a west-east direction parallel to the depression. The area of cultivated

lands as for September 2013 is estimated at 346 km^2 (85,498 acres), which represents 28% of the total area of the Dakhla depression (Fig. 4).

Soil salinity across the depression ranges from 2dS/m to more than 73dS/m. Soils having salinity lower than 10 dS/m represent 11.2% of the total samples. Average soil salinity for the collected 66 samples is 32.54 dS/m, median is 32.7 dS/m, mode is 36.2 dS/m, standard deviation is 17.34 dS/m, 25^{th} percentile is 22.4 dS/m, 50^{th} percentile is 32.7 dS/m and the 75^{th} percentile is 39.5 dS/m. The majority of the collected soils have sandy texture, however, little samples have silty and clayey sandy texture. Regression models produced for soil salinity using the OLI image are shown in Table (2). Fifteen models reveal positive regression correlations and the other three (B3/B5, B3/B6 and B4/B3) provide negative correlations. The lowest regression coefficient (R^2) is encountered for B6/B3 index ($R^2 = 0.0722$), while the highest R^2 is observed for the TC brightness transform ($R^2 = 0.5395$). Consequently, the TC model is used to prepare a salinity map of the depression. The model applies the equation $y = 250.57x + 31855$, where x is the predicted soil salinity of each pixel in dS/m and y is the value of that pixel in the TC brightness component. Figure 5 represents the locations and ranges of salinity levels in the depression. The area of bare and fallow soils is 427 km^2 (34% of the depression); of which non-saline soils (<4 dS/m) occupy only 38 km^2 (9% of bare and fallow lands). Soils having salinity levels of 4-12, 12-20, 20-28, and more than 28 dS/m represent 105, 98, 99, and 88 km^2, respectively. The majority of salt-affected soils occur within the middle micro-depression. The remaining land of the depression (467 km^2) is generally covered by mobile sand dunes, sand sheets and surface lakes from agricultural drainage.

Satellite images reveal that two types of sand dunes dominate across Dakhla depression. The linear dunes occur north of the escarpment and are aligned to the net trend of sand drift (Fig. 6), whereas simple (isolated) to compound (coalesced) barchan dunes mostly prevail south of the escarpment and along the western side of the depression. Rates of dune advance as measured for two brilliant groups of barchan dunes (Fig. 7) show different movements between those occurring at the open upland north of the escarpment and those running at the depression floor in the lee side of the escarpment. Satellite data visualized by Google Earth reveal that dunes at the northern plateau moved faster than those within the depression. The barchan in the sand dune field 1 advanced at a rate of 5.9 m/y, whereas and the barchan in the sand dune field 2

moved at a rate of 3.6 m/y between 2002 and 2013 (Fig. 7). These results are comparable with a previous estimation of dune advance rate in Dakhla that ranges from 3 to 6 m/y (Ghadiry et al. (2012).

5. Discussion

The discrepancy between spectral behavior of the green vegetation and salt-affected soils could help discriminate salts in soils quantitatively using satellite images. The spectral signature curves for these two land features (Fig. 8) reveal a conspicuous difference in the visible and infrared portions of the spectrum. Green vegetation considerably absorbs red light at the time where salt-affected soils reflect as much as 50% of the this light. On the other hand, although the NIR is reflected equally from the two land features, the light is reflected much greater in the SWIR bands from salt-affected soils than from the green vegetation. Applying suitable spectral indices, such as SAVI is, therefore, effective to distinguish each of these landforms individually. Landsat images have the potential to map regional distribution of soil salinity. Individual bands in the OLI image showed high correlations with soil salinity, particularly the red and the SWIR bands, which is supported by previous studies (Dwivedi & Rao, 1992; Metternicht & Zinck, 1997). However, the application of band algebra yields better correlations (e.g. B3/B4 and B3/B6). Maximum regression coefficient ($R^2 = 0.5395$) is observed when the TC transform was applied. The premise is that all bands in this transformation are multiplied by specified constants (Kauth, & Thomas, 1976) and the resultant model can augment the reading of the red and SWIR bands, which significantly correlate with salt crusts of bright soils (Dwivedi & Rao, 1992).

Soil degradation by salinization in Egypt's vast deserts is one of the problems that has recently received attention for research (Masoud and Koike, 2006; Nawar et al., 2014). Drought, which is a natural phenomenon, is a significant driving force for soil degradation in the Western Desert of Egypt as precipitation is much less than evapotranspiration rates. According to the classification of arid lands (UNESCO, 1979), hyper-arid regions have aridity index (P/ETP) of <0.03, where P is the precipitation and ETP is the evapotranspiration. Dakhla region has an aridity index of <0.001 (Table 1), which is far less than the limit of hyper-arid regions (P/ETP < 0.03). The high groundwater table could be another reason triggering soil salinization (Chhabra, 1996). The depression occurs upon the massive Nubian groundwater

aquifer. This sandstone water system extends throughout the entire southern part of the Western Desert for a thickness of 2500 m (Shata, 1982). The aquifer is overlain by a thick clay layer, which acts as an aquiclude, allowing water to be under confined to semi-confined conditions (Ebraheem et al., 2004) and water somewhere flows into the surface through fractures and rock joints. High evaporation rates in the region allow for increasing salt concentrations at the soil surface. Soil salinization is also attributed to human activities, notably the abuse of water resources. The irrigation practices in Dakhla is one important reason for human-induced (secondary) salinization. Although water salinity of the groundwater aquifer in Dakhla is around 500 ppm (Soltan, 1999), which is fairly good for irrigation, traditional methods for irrigation are not quite suitable due to the arid climate. The lack of a well developed drainage system lead to recharging groundwater with agricultural drainage to the degree that the water table occurs at the surface (Fig. 9). At the same time drainage water seeps to low-land regions in the depression forming artificial lakes, such as Lake Mut. Impacts of this severe salinization involve not only the destruction of soil physical structure but also impairing the soil ecosystem as well. Soil dispersion and other engineering problems are direct impacts (Metternicht and Zinck, 2003), whereas toxicity of microorganisms and mortality of domestic vegetation are inevitable (Keren 2000).

The absence of natural vegetation cover due to drought conditions is a prompting factor for making sands to be exposed to the wind action. The source of sand in this region is the Great Sand Sea in the north, where sustainable sand supply accompanied by continuous stream of northwesterly wind dragging across open and bare desert are the main factors affecting the sand drift. Satellite images reveal that sand dunes are more abundant north of Abu Tartur escarpment than within the depression floor, which may be attributed to the blocking effect of the escarpment. Moreover, the major dune type in the upland area north of the depression is the linear type, where the axes of the dunes are parallel to the trend of the dominant wind (Hereher, 2010). Linear dunes usually move slowly as the single dune could extend to more than 100 km long, hence they appear as stabilized in satellite images. However, through the western part of the depression, where the escarpment narrows, dunes are funneled and cascade through the lower part of the escapement into the depression. At the west, the threat of sand encroachment is significant and the hazards are manifested at cultivated lands, settlements and roads (Fig. 6). The northern escarpment also

reduces the wind energy passing across the depression, which is revealed by the slowing of the dune advance rates from 5.9 m/y in the upland north of the escarpment to 3.6 m/y in the depression. Hereher (2010) reported that the wind regime of the Dakhla meteorological station belongs to the low-energy wind environment and the annual volumetric amount of sand drift approach 2.17 m^3/m. Although the sand drift and dune advance rates in the Dakhla depression are lower than in the surrounding desert, these dunes cause considerable problems to soil fertility by increasing the sand fraction of the soil texture and by the accumulation upon cultivated crops and reclaimed areas. Sand fences, such as locally grown palm leafs are highly recommended in the sandy corridors west of the depressions. Fences were efficient to suppress sand drift in similar areas (Alghamdi & Al-Kahtani, 2005).

6. Conclusions

This paper investigated the application of multi-temporal remote sensing data and regression model in conjunction with TC transformer to diagnose the severity of dune advance and soil salinity in the Dakhla depression. From this study, the following conclusions were made: 1- the sand dunes in Dakhla are active and sand encroachment is a significant natural hazard due to the occurrence of the depression along the downwind side of the major sand sea in the Western Desert. However, the northern escarpment of the depression protects the region from moving sand dunes except for the western side of the depression, where the escarpment is narrow and dunes could cascade to threat cultivated lands and infrastructures. 2- sources of soil salinization in the depression are primary (climatic and topographic factors) and secondary (poor drainage). 3- this study demonstrates that remote sensing techniques are important to acquire regional information for remotely desert areas. The tasseled cap (TC) transform is most suitable to map soil salinity and it recommended to be applied in similar desert regions. The prolonged drought conditions concomitant with human abuse of water resources could accelerate desertification, which is most obvious by soil salinization more than sand drift. 4- detailed studies are recommended to characterize physico-chemical properties and salt types in the soil. Understanding the characteristics and driving forces of salinization and sand encroachment could help prepare suitable management of water resources, soil and cultivated lands.

Acknowledgements

The authors would like to thank and appreciate the deep revision, comments and suggestions of the anonymous reviewers that improved of the manuscript.

References

Alghamdi AA and Al-Kahtani NS. 2005. Sand Control Measures and Sand Drift Fences. J Performance of Constructed Facilities. 19 (4): 295-299.

Beaumont P. 1993. Climate and hydrology. In: G. Craig (ed): The agriculture of Egypt. Oxford University Press, pp. 17-38.

Breed CS & Grow T. 1979. Morphology and distribution of dunes in sand seas observed by remote sensing. In E. D. McKee (Ed.), United States geological survey professional paper: Vol. 1052. A study of global sand seas (pp. 253-304). Washington DC.

Central Laboratory for Agricultural Climate (CLAC). 2015. Summaries of climatic normals. The Ministry of Agriculture, Dokki, Cairo - Egypt (www.clac.edu.eg).

Chavez PS. 1996. Image-based atmospheric correction—revised and improved. Photogrammetric Engineering and Remote Sensing. 62:1025–1036.

Chhabra R. 1996. Soil salinity and water quality. Balkema Pub., VT, USA.

Darwish Kh & Abdel Kawy WA. 2008. Quantitative Assessment of Soil Degradation in some Areas North Nile Delta, Egypt. Int J Geology. 2: 17-22.

Dellavalle NB. (ed.). 1992. Determination of soil-paste pH and conductivity of saturation extract, pp. 40-43 In Handbook on Reference Methods for Soil Analysis. Soil and Plant Analysis Council, Inc. Athens, GA.

Dwivedi RS & Rao BR. 1992. The selection of the best possible Landsat TM band combination for delineating salt-affected soils. Int J Rem Sens. 13: 2051–2058.

Dwivedi RS. 1992. Monitoring and the study of the effects of image scale on delineation of salt-affected soils in the Indo-Gangetic alluvial plains. Int J Rem Sensing. 13:1527–1536.

Ebraheem MA, Riad S, Wycisk P and Sefelnasr AM. 2004. A local-scale groundwater flow model for groundwater resources management in Dakhla Oasis, SW Egypt. Hydrogeology Journal. 12:714–722.

Elmahdy SI and Mohamed MM. 2015a. Remote sensing and geophysical survey applications for delineating near-surface palaeochannels and shallow aquifer in the United Arab Emirates. Geocarto International, DOI:10.1080/10106049.2014.997306

Elmahdy SI and Mohamed MM. 2015b. Groundwater of Abu Dhabi Emirate: a regional assessment by means of remote sensing and geographic information system. Arabian Journal of Geosciences, DOI:10.1007/s12517-015-1932-2.

Elmahdy SI, Mohamed MM and Marghany MM. 2015. Mapping and classification of hydrological parameters from digital terrain data in the Musandam Peninsula, UAE and Oman. Geocarto International, DOI:10.1080/10106049.2014.965755

FAO/UNESCO 1977. Soil map of the world at a scale of 1:5,000,000, Vol.6, Africa. UNESCO, Paris.

Fernandez-Bucesa N, Siebea C, Cramb S and Palacio JL. 2006. Mapping soil salinity using a combined spectral response index for bare soil and vegetation: A case study in the former lake Texcoco, Mexico. J Arid Environ. 65: 644–667.

Fryberger SG, Al-Sari A, Clishman TJ, Rizvi SA, Al-Hinai KG. 1984. Wind sedimentation in the Jafurah sand sea, Saudi Arabia. Sediment. 31: 413-431.

Ghadiry M, Shalaby A, Koch B. 2012. A new GIS-based model for automated extraction of Sand Dune encroachment case study: Dakhla Oases, western desert of Egypt. The Egyptian J Rem Sensing and Space Sciences. 15: 53–65.

Hereher M, Salem . and Abdel Hamid H. 2010. Change Detection of Salt-Affected Soils at the Coastal Zone of the Nile Delta Using Remote Sensing. Egyptian Journal of Soil Sciences. 50: 111-123.

Hereher M. 2010. Sand movement patterns in the Western Desert of Egypt: an environmental concern. Environ Earth Sciences. 59: 1119-1127.

Hereher M. 2014. Assessment of sand drift potential along the Nile Valley and Delta using climatic and satellite data. Applied Geography. 55: 39-37.

Hereher M. 2015. Environmental monitoring and change assessment of Toshka lakes in southern Egypt using remote sensing. Environ Earth Sci. 73: 3623-3632.

Huete A. 1988. A soil-adjusted vegetation index (SAVI). Remote Sensing of Environment, 25:295–309

Hugenholtz CH, Levin N, Barchyn TE, Baddock MC. 2012. Remote sensing and spatial analysis of aeolian sand dunes. Earth-Science Reviews. 111: 319–334.

Judkins G, Myint S. 2012. Spatial Variation of Soil Salinity in the Mexicali Valley, Mexico: Application of a Practical Method for Agricultural Monitoring. Environmental Management, 50, 478–489.

Kassas M. 1987. Drought and desertification. Land Use Policy, 4, 389-400.

Kauth RJ, Thomas GS. 1976. The tasseled Cap - A graphic description of the spectral-temporal development of agricultural crops as seen by LANDSAT. Proceedings of the Symposium on Machine Processing of Remotely Sensed Data, Purdue University of West Lafayette, Indiana, 1976: 4B-41 to 4B-51.

Keren R. 2000. Salinity, Chapt 1. In: Sumner ME (ed) Handbook of soil science. CRC Press, New York, pp G3–G25

Knight M, Thomas DS, Wiggs GF. 2004. Challenges of calculating dunefield mobility over the 21st century. Geomorphology. 59: 197–213.

Lancaster N. 2009. Dune morphology and dynamics. A.J. Parsons, A.D. Abrahams (eds.), Geomorphology of Desert Environments, 2nd ed., Springer Science + Business Media B.V.

Livingstone I, Wiggs G, Weaver C. 2007. Geomorphology of desert sand dunes: A review of recent progress. Earth-Science Reviews. 80: 239–257.

Masoud AA and Koike K. 2006. Arid land salinization detected by remotely-sensed landcover changes: A case study in the Siwa region, NW Egypt. Journal of Arid Environments. 66: 151–167.

Metternicht GI, Zinck JA. 1997. Spatial discrimination of salt-and sodium-affected soil surfaces. International Journal of Remote Sensing. 18: 2571-2586.

Metternicht GI, Zinck JA. 2003. Remote sensing of soil salinity: potential and constraints. Remote Sensing of Environment. 85: 1-20.

Misak RF, Draz MY. 1997. Sand drift control of selected coastal and desert dunes in Egypt; case studies. Journal of Arid Environments. 35: 17-28.

Mohamed ES, Morgun EG, Goma B. 2011. Assessment of soil salinity in the eastern Nile Delta (Egypt) using geoinformation techniques. Moscow University Soil Science Bulletin. 66: 11–14.

Mougenot BM, Epema G. 1993. Remote sensing of salt-affected soils. Remote Sensing Reviews. 7: 241-259.

Nawar S, Buddenbaum H, Hill J, Kozak J. 2014. Modeling and Mapping of Soil Salinity with Reflectance Spectroscopy and Landsat Data Using Two Quantitative Methods (PLSR and MARS). Rem Sens. 6: 10813-10834.

Piper C. 1955. Soil and plant analysis. A laboratory manual of methods for examination of soil and determination of inorganic substitution of plant. New York Int. Pub. Inc., USA; 1955.

Rao B, Sankar T, Dwivedi R, Thammappa SS, Venkataratnam L, Sharma RC, Das SN. 1995. Spectral behavior of salt-affected soils. International Journal of Remote Sensing. 16: 2125-2136.

Sadek Sh. 1993. Use of Landsat imagery for monitoring agricultural expansion of east and west Nile Delta, Egypt. Egyptian Journal of Soil Science. 33: 23-33.

Shata AA. 1982. Hydrogeology of the great Nubian sandstone basin, Egypt: Quarterly Journal of Engineering Geology. 15: 127-133.

Soltan M. 1999. Evaluation of groundwater quality in Dakhla Oasis (Egyptian Western Desert). Environmental Monitoring and Assessment. 57: 157–168.

Sparavigna AC. 2013. A Case Study of Moving Sand Dunes: The Barchans of the Kharga Oasis. International Journal of Sciences. 2: 95-97.

Sumner ME. 2000. Handbook of Soil Science. CRC Press, Boca Raton, FL, USA.

Tchakerian VP. 1999. Dune palaeoenvironments. In: Goudie, A.S., Livingstone, I., Stokes, S. (Eds.), Aeolian Environments, Sediments and Landforms. Wiley, Chichester, pp. P292– P361.

Tolba MK. 1986. Desertification in Africa. Land Use Policy. 3: 260-268.

Tucker C. 1979. Red and photographic infrared linear combination for monitoring green vegetation. Remote Sensing of Environment. 8: 127 - 150.

UNESCO 1979. Map of the World Distribution of Arid Regions. MAB Technical Note 7.

United Nations Environment Program (UNEP) 1991. Status of desertification and implementation of the United Nations Plans of action to combat desertification. UNEP, Nairobi.

United Nations Environment Program (UNEP) 1992. World atlas of desertification. Edward Arnold, Seven Oaks, UK.

Yao ZY, Wang T, Han ZW, Han WM, Zhao AG. 2007. Migration of sand dunes on the northern Alxa Plateau, Inner Mongolia, China. J Arid Environ. 70: 80–93.

Table (1): Climatic parameters of Dakhla meteorological station. P is the Precipitation, ETP is the Evapotranspiration and T is the Temperature. Source: Central Laboratory for Agricultural Climate, the Ministry of Agriculture (www.clac.edu.eg).

Month	P, Mm	ETP, mm/d	T, C°	Humidity %	Wind speed, knots
Jan.	0.1	2.6	12.0	41	3.2
Feb.	0.2	3.5	14.0	34	3.8
Mar.	0.0	5.0	18.1	26	4.3
Apr.	0.1	6.6	23.5	20	4.6
May	0.1	8.1	27.5	19	5.2
Jun.	0.0	9.0	30.7	20	5.5
Jul.	0.0	8.5	30.9	23	4.4
Aug.	0.0	8.0	30.5	24	4.8
Sep.	0.0	7.2	28	29	4.2
Oct.	0.0	5.5	24.3	32	3.8
Nov.	0.0	3.7	18.5	40	3.0
Dec.	0.0	2.6	13.6	42	3.0

Table (2): Regression models operated to correlate salinity with OLI pixel values either as individual bands, band algebra, or band transformation. TC_Brightness refers to the tasseled cap transformation 1 (brightness component).

Spectral band/algebra	Regression Model	Regression Coefficient, R^2
B1 (Blue)	Y = 46.801x + 11079	0.2271
B2 (Green)	Y = 88.134x + 11097	0.3435
B3 (Red)	Y = 142.19x + 11785	0.3923
B4 (NIR)	Y = 85.674x + 19357	0.3402
B5 (SWIR1)	Y = 216.63x + 15740	0.3727
B6 (SWIR2)	Y = 214.2x + 11394	0.3858
B3/B4	Y = 0.0034x + 0.6284	0.2367
B3/B5	Y = -0.0015x + 0.7862	0.0462
B3/B6	Y = -0.0042x + 1.0691	0.1375
B4/B3	Y = -0.0066x + 1.5995	0.2385
B5/B3	Y = 0.0019x + 1.3271	0.0174
B6/B3	Y = 0.0038x + 0.9885	0.0722
B1*B3	Y = 2.6298x + 124.85	0.3474
B3*B4	Y = 4.832x + 211	0.4179
B3*B6	Y = 6.4076x + 105.41	0.4286
(B6-B1)/(B6+B1)	Y = 0.0042x + 0.0296	0.3729
(B5-B3)/(B5+B3)	Y = 0.0011x + 0.0397	0.3385
TC_Brightness	Y = 250.57x + 31855	0.5395

Figure (1): Location map showing the Dakhla depression at the Western Desert of Egypt.

Figure (2): Soil sampling sites and selected dune fields across the Dakhla depression.

Figure (3): Painted relief map of Dakhla obtained from the DEM with three discontinuous hollows of low-lands surrounded by a northern escarpment and a southern plateau.

Figure (4): The extent and distribution of cultivated lands in 2013 as obtained from the SAVI algorithm that applied to the Landsat-8 OLI image.

Figure (5): A salt-affected soil map of Dakhla highlighting the distribution of the different soil salinity levels along the depression as obtained from the regression model (top) and the area as well as the percent of occurrence of each salinity level (bottom) derived from the TC model.

Figure (6): Dune forms of the Dakhla region as appear in the OLI image (top) with the dominance of linear dunes that occur parallel to the net wind direction. The rose diagram in the satellite image is adopted from Hereher (2010). The bottom pictures show the encroachment of dunes upon roads and cultivated lands.

Figure (7): A Google Earth view (1:5000) of two dune fields north (top) and south (bottom) of Abu Tartur Plateau. At each dune field, the location of a brilliant barchan dune is compared in 2013 with its location in 2002. Note that the dunes in the northern field were faster than those in the southern field.

Figure (8): Spectral signature curves for salt-affected soils and green vegetation.

Figure (9): Ground pictures of Dakhla depression; a) a salt crust at a barren soil area, b) Lake Mut with its margins affected by salinization, c) the mortality of date palms from soil salinization, and d) higher water table severely impacted vegetation with high salinity.